Dear Author,

Please, note that changes made to the HTML content will be added to the article before publication, but are not reflected in this PDF.

Note also that this file should not be used for submitting corrections.

Chemical Physics Letters xxx (2015) xxx–xxx

Contents lists available at ScienceDirect

Chemical Physics Letters

journal homepage: www.elsevier.com/locate/cplett

Structure, magnetism, and dissociation energy of small bimetallic cobalt-chromium oxide cluster cations: A density-functional-theory study

Q1 Hung Tan Pham[a,b], Ngo Tuan Cuong[c], Nguyen Minh Tam[b,d], Vu Dinh Lam[a], Nguyen Thanh Tung[a,*]

[a] Institute of Materials Science, Vietnam Academy of Science and Technology, Viet Nam
[b] Institute for Computational Science and Technology, Viet Nam
[c] Center for Computational Science, Hanoi National University of Education, Viet Nam
[d] Department of Chemistry, KU Leuven, B-3001 Leuven, Belgium

ARTICLE INFO

Article history:
Received 4 October 2015
In final form 13 November 2015
Available online xxx

ABSTRACT

We study $Co_xCr_yO_m^+$ ($x+y=2$, 3 and $1 \le m \le 4$) clusters by means of density-functional-theory calculations. It is found that the clusters grow preferentially through maximizing the number of metal–oxygen bonds with a favor on Cr sites. The size- and composition-dependent magnetic behavior is discussed in relation with the local atomic magnetic moments. While doped species show an oscillatory magnetic behavior, the total magnetic moment of pure cobalt and chromium oxide clusters tends to enhance or reduce as increasing the oxygen content, respectively. The dissociation energies for different evaporation channels are also calculated to suggest the stable patterns, as fingerprints for future photofragmentation experiments.

1. Introduction

During the last decades, transition metal (TM) oxide clusters have been investigated extensively, revealing a non-monotonic dependence of physical and chemical properties on the number of constituent atoms and the cluster composition [1–3]. Their structures, chemical reactivities, ionization potentials, dissociation energies, magnetic moments, and energetic formations thus become interesting subjects and challenging to understand [4,5]. While the earlier work mainly concentrated on mono-TM oxide clusters, alloy species have been explored later in the quest for building blocks of novel nanostructured materials. Advanced production techniques in combination with the knowledge of electronic and geometric structures allow us to design, produce, and manipulate size- and composition-selected TM oxide clusters for probing interesting physical properties [6]. For instance, geometric structures of singly TM (TM = Sc, Ti, Cr or Co) for V substituted $(V_2O_5)_{n-1}(VTMO_5)^-$ ($n=2$–4) cluster were found identical to those of their isoelectronic counterparts, the neutral $(V_2O_5)_n$ clusters [7–9]. The electronic structures of $MM'O_7^{2-}$ and $M_2O_7^{2-}$ (M, M′ = Cr, Mo, and W) clusters were altered by changing their composition and charge state [10]. The composition dependent electronic and geometric structures of $MM'O_{2-5}^-$ (M, M′ = Mo, V, Al, and W) clusters were discussed by means of vibrationally resolved anion photoelectron spectroscopy and density functional theory (DFT) calculations [11–13]. The same approach was applied to analyze the impact of spin contamination in the series of heteronuclear $MoNbO_y^-$ ($y=2$–5) transition metal oxide clusters [14]. The electron transfer and the geometric structures of $[(CeO_2)(VO_2)_{1-2}]^+$ and $[(Ce_2O_3)(VO_2)]^+$ clusters were discussed using infrared vibrational pre-dissociation spectroscopy experiments and quantum chemical computations [15]. Structural, vibrational, and magnetic properties of neutral and ionized oxides of the magnetic dimer FeCo as a function of the oxygen content $FeCoO_n^{0,+}$ ($n=1$–6) were investigated by means of DFT calculations [16]

On the other aspect, the magnetic phenomenon of TM related oxide systems have attracted considerable attention. A particular interest has been paid for TM doped TiO_2 and ZnO [17,18] to synthesize diluted magnetic semiconductors. Recent studies have shown that the *p–d* exchange can be replaced by *p–p* coupling interactions in non-metal doped species to induce ferromagnetic behavior [19–21]. The possibility of oscillatory *d–d* exchange couplings have been reported in reduced-size TM oxide systems by varying localized electronic states [22]. Among of TM elements,

* Corresponding author.
E-mail address: tungnt@ims.vast.ac.vn (N.T. Tung).

http://dx.doi.org/10.1016/j.cplett.2015.11.015
0009-2614/

Co and Cr oxide clusters likely have interesting magnetic properties. Preliminary studies showed that the oscillatory magnetic interactions between the local magnetic moments of chromium oxide clusters can be altered by varying the oxygen concentration [23]. On the other hand, bulk cobalt–chromium oxide systems attract significant attention owing to their promising magnetoelectric properties, in particular the multiferroic spinel $CoCr_2O_4$, which exhibits simultaneously ferroelectricity and ferromagnetism [24–26]. It suggests that introducing magnetic dopant atoms in TM oxide clusters might offer the possibility to simultaneously manipulate the geometrical structure and oscillations of the magnetic exchange coupling, resulting in ferromagnetic, ferrimagnetic, or even non-magnetic species with enhanced stability. Nevertheless, the magnetism in cluster-based nano-materials, where the lateral island sizes are reduced to dimensions that might even be smaller than the typical magnetic domain sizes, has not been completely understood yet. In order to bridge this gap, studies of their atomic-scale structures, stability, and magnetic properties are indispensable.

In our recent investigation, the evolution of the geometric structure and relative stability of singly Cr doped Co oxide clusters, $Co_{n-1}CrO_m^+$ ($n = 2$, 3; $m = 2$–6 and $n = 4$; $m = 3$–8), were investigated using DFT calculations and photodissociation spectroscopy [27]. A good agreement between experimental and simulation results was achieved. Nevertheless, a systematic study on structures and stability of Co–Cr oxide clusters with higher Cr concentration has not been reported yet. Moreover, insight into the size- and constituent-dependent magnetism of cobalt–chromium oxide clusters may eventually guide further Stern–Gerlach experiments [28–30] on tailoring the functionality of potential cluster-based multiferroics. Being motivated by successful combination with future photodissociation and magnetic deflection experiments, we set out to systematically investigate the dependence of the structures, dissociation energies, and magnetism of $Co_xCr_yO_m^+$ ($x+y = 2$, 3 and $1 \le m \le 4$) cluster cations on their size and composition using DFT calculations. The following parts of this Letter is organized as follows. Section 2 describes the used computational method. The results and discussions are presented in Section 3. In particular, the ground state structures of $Co_xCr_yO_m^+$ are investigated in Section 3.1 while Section 3.2 discusses the alloying effect on magnetic behavior of Co–Cr oxide clusters. In Section 3.3, dissociation energies for different evaporation channels and relative stability are reported in comparison with the available theoretical/experimental data. The conclusion is made in the final section.

2. Methodology

For all calculations, we have used the hybrid B3P86 functional [31,32] in conjunction with the cc-pVTZ and cc-pVTZ-pp (pp stands for a set of pseudo-potentials) basis sets as implemented in the GAUSSIAN 09 program [33]. Symmetric-unrestricted optimization is carried out at the B3P86/cc-pVTZ-pp level for Co and Cr and the B3P86/cc-pVTZ level for O. The 3*d* and 4*s* electrons of Co and Cr are treated as valance electrons. The searches for energy minima are conducted using different approaches. Firstly, a stochastic genetic algorithm is applied to generate all possible structures [34]. The equilibrium structures that are initially detected using low-level computations, are re-optimized using a higher level method. In the second approach, initial structures of clusters $Co_xCr_yO_m$ are manually constructed by either interchanging the positions of Co atoms and Cr atoms, or adding one O atom at various positions on structures of the $Co_xCr_yO_{m-1}$ clusters. In addition, the local energy minima of Co_xO_m and Cr_yO_m clusters previously reported are also used as referenced structures. Relative energies of the lowest isomers and dissociation energies are determined on the basis of single-point calculations for the optimized structures using the full electron cc-pVTZ basis set. We have also considered all possible spin multiplicities for each of these structures, ensuring the robustness of the ground-state search. For structure optimization and energy calculations, the energy, gradient, and displacement tolerance are 2.0×10^{-5} hartree, 4×10^{-3} hartree/Å, and 5×10^{-3} Å, respectively.

Table 1
Calculated bond lengths, spin states, and dissociation energies of CoO, CoO^+, CrO, CrO^+, and O_2 dimers obtained using different functionals in conjunction with both cc-pVTZ and cc-pVTZ-pp (values in the parentheses) basis sets and comparison with available theoretical/experimental values.

Dimer	Method	*R* (Å)	*M*	DE (eV)
CoO/CoO^+	B3P86	1.57/1.61	4/5	3.78 (3.72)/3.00 (3.16)
	B3LYP	1.59/1.63	4/5	3.60 (3.54)/2.88 (3.06)
	B3PW91	1.58/1.62	4/5	3.58 (3.52)/2.86 (3.04)
	PBEPBE	1.62/1.62	4/5	4.96 (5.06)/4.14 (4.26)
	Theo.	1.59[a]/1.63[b]	4[b]/5[b]	4.97[b]/4.13[b]
	Exp.	1.63[c]/–	–/–	3.94[d]/3.24[d]
CrO/CrO^+	B3P86	1.60/1.58	5/4	4.38 (4.40)/3.12 (3.16)
	B3LYP	1.61/1.59	5/4	4.36 (4.40)/3.08 (3.10)
	B3PW91	1.61/1.59	5/4	4.10 (4.12)/2.86 (2.90)
	PBEPBE	1.61/1.57	5/4	5.20 (5.16)/4.34 (4.32)
	Theo.	1.61[e]/–	5[e]/–	4.33[e]/–
	Exp.	1.61[f]/–	5[f]/–	4.38[d]/–
O_2	B3P86	1.20	3	5.53
	B3LYP	1.20	3	5.27
	B3PW91	1.20	3	5.32
	PBEPBE	1.22	3	6.16
	Theo.	1.22[b]	3[b]	6.18[b]
	Exp.	1.21[d]	–	5.17[d]

[a] Ref. [35].
[b] Ref. [36].
[c] Ref. [37].
[d] Ref. [38].
[e] Ref. [39].
[f] Ref. [40].

To check the accuracy of the used level we first perform the calculations on CoO, CoO^+, CrO, CrO^+, and O_2 dimers, which are listed in Table 1. Calculated bond lengths (*R*), spin states (*M*), and dissociation energies (DEs), obtained using different functionals in conjunction with the cc-pVTZ and cc-pVTZ-pp (values in the parentheses) basis sets, are compared with each other and with available theoretical/experimental values. It can be seen that the computational results are in in-line with the values in literature. There is almost no difference between the values obtained by cc-pVTZ and cc-pVTZ-pp basis sets. The calculated bond lengths are very close to the measured ones. The DEs of oxide dimers, calculated using B3PW91 and PBEPBE, slightly underestimate and overestimate the experimental values, respectively, while those obtained by B3P86 and B3LYP are well matched with the measurement data. The ground-state spin configurations of the neutral and cationic oxide dimers also well agree with previous studies. These excellent agreements between the calculated and experimental data suggest the reliability of our computational approach employed in the present work.

3. Results and discussion

3.1. Equilibrium geometries

Figure 1 presents the equilibrium structures of $Co_xCr_yO_m^+$ ($x+y = 2$, 3 and $m = 1$–4) clusters. Although a number of different geometry and spin configurations are identified for each stoichiometry, only the lowest-energy isomers are discussed. Detailed descriptions of other isomers with different geometries and

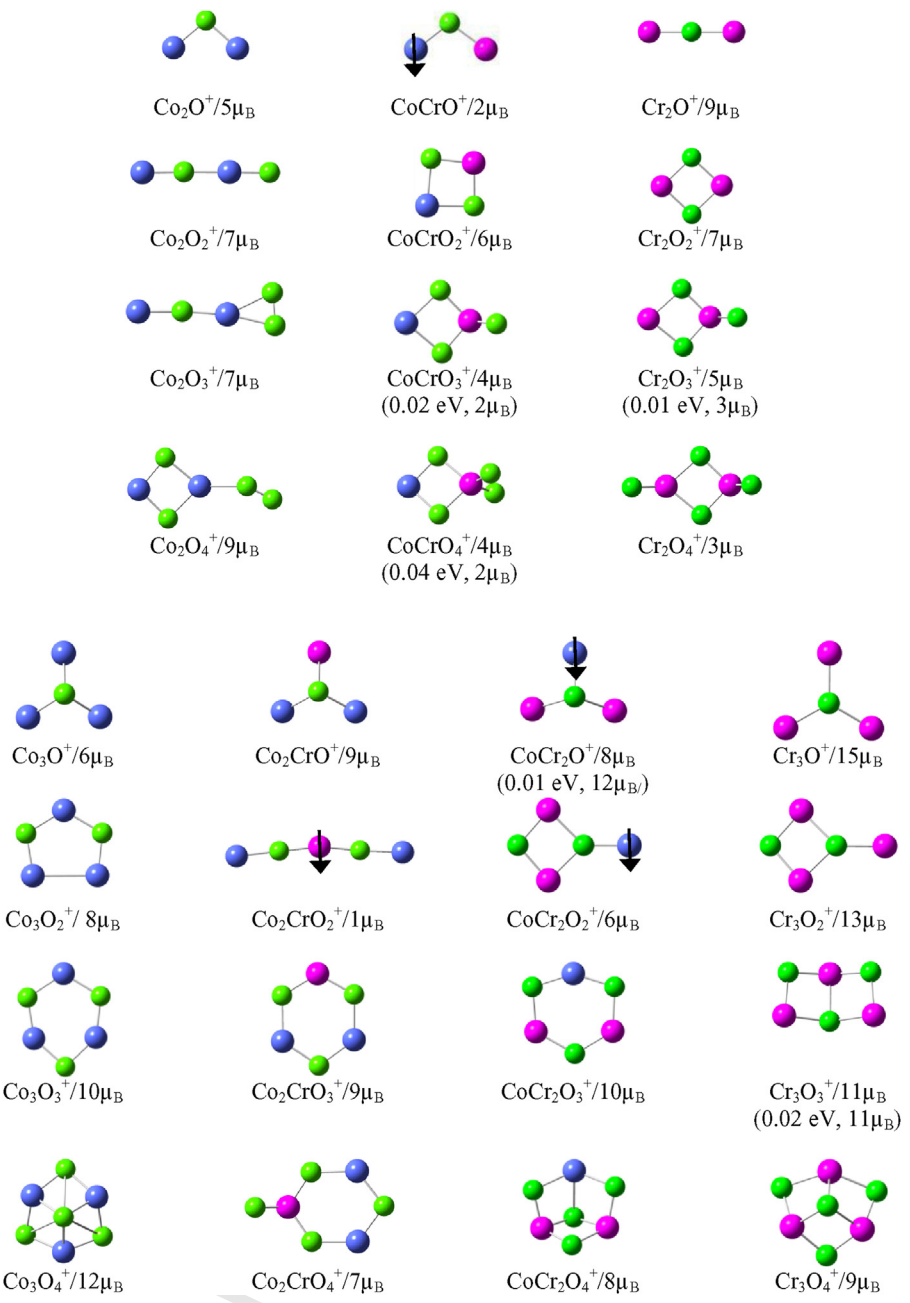

Figure 1. Optimized structures and total magnetic moments of $Co_xCr_yO_m^+$ ($x+y=2$, 3 and $m=1$–4) clusters. The green, blue, and magenta spheres represent O atoms, Co atoms, and Cr atoms, respectively. The values in parentheses indicate the difference in total energy from the corresponding ground state and the total magnetic moment of isomers. The arrows indicate the antiparallel relation of the local magnetic moment to others. (For interpretation of reference to color in this figure legend, the reader is referred to the web version of this article.)

magnetic moments are provided in our Supplementary Material [41]. In line with the previous observations [22,23,35–37], the present calculations on cobalt–chromium oxide clusters confirm the well-defined growth mechanism that is to maximize the number of oxygen-metal bonds. Generally, the oxidization process can be divided into two stages: (i) the first oxygen atoms occupy the bridging positions and then (ii) the next oxygen atoms bind atop/aside metal atoms. The preference of metal–oxygen bonds can be interpreted by the larger metal–oxygen binding energies (3.78 eV for Co–O and 4.38 eV for Cr–O) over those of metal–metal ones (2.9 eV for Co–Co [42] and 1.64 eV for Co–Cr [43]). For doped species, oxygen atoms favor to form Cr–O bonds rather than Co–O one, being consistent with the larger binding energy of CrO dimer compared to that of CoO one.

In particular, the mono-oxide Co_2O^+ and $CoCrO^+$ clusters select the triangle as the most stable structure while Cr_2O^+ energetically favors a chain form. The difference is more obvious for higher oxygen-concentration species. The linear chain found for ground state $Co_2O_2^+$ is less expected in comparison with the early predicted ring structure [36,44], which, nevertheless, requires a relative energy of +1.30 eV in our calculations. The most stable structure of $Co_2O_3^+$ is formed by an additional oxygen atom attaching to the Co site of $Co_2O_2^+$ chain. Pure chromium dioxide $Cr_2O_2^+$ cluster prefers a four-membered ring geometry, which is in agreement with previous reports for the ring-based motif of dichromium oxides [22,45]. Additional oxygen atoms likely attach to the saturated metal–oxygen framework $Cr_2O_2^+$ rather than promote a structural transformation, for instance, in $Cr_2O_3^+$ and $Cr_2O_4^+$.

Please cite this article in press as: H.T. Pham, et al., Chem. Phys. Lett. (2015), http://dx.doi.org/10.1016/j.cplett.2015.11.015

This tendency is very similar to what observed in neutral Cr_2O_m ($m = 1$–6) clusters by Reddy and Khanna [22]. In contrast, the equilibrium structure of $Co_2O_4^+$ is based on a $Co_2O_2^+$ ring instead of the linear form, with an additional oxygen molecule weakly bonded to the Co site. The greater binding energy of the Cr–O bond over that of the Co–O one obviously influences the structure of doped clusters: alloying species prefer the ring-based motif ($CoCrO_2^+$) with surface-adsorbed oxygen atoms ($CoCrO_3^+$ and $CoCrO_4^+$). Unlike in $Cr_2O_4^+$, two surface-adsorbed oxygen atoms in $CoCrO_4^+$ prefer binding to the Cr site only, which is again attributed to the larger binding energy of CrO dimers compared to that of CoO ones.

All ground-state structures of the group $x+y=3$ favor maximizing metal–oxygen bonds. For instance, the lowest-energy structures of all mono-oxide species have three metal–oxygen bonds, forming a triangular pyramid with the oxygen atom bridging three metal atoms. The ground state $Co_3O_2^+$ favors the five-membered ring geometry while $Co_2CrO_2^+$ has the linear chain equilibrium structure. The minimum-energy structure of $CoCr_2O_2^+$ or $Cr_3O_2^+$ is a four-membered Cr–O–Cr–O ring with the third metal atom weakly bonded to the O site. A six-membered ring unit is found to be the most stable isomer of $Co_3O_3^+$, $Co_2CrO_3^+$, and $CoCr_2O_3^+$. The structure of $Cr_3O_3^+$ degenerates into a double square ring (ground state) and again a six-membered ring (+0.02 eV). The next oxygen atom prefers to be adsorbed to the stable ring unit, for instance, in the cases of $Co_3O_4^+$, $Co_2CrO_4^+$, $CoCr_2O_4^+$, and $Cr_3O_4^+$. This finding is supported by earlier calculations on the structures of $Cr_3O_6^+$ and $Cr_3O_7^+$, which are also formed by a $Cr_3O_3^+$ ring with three and four attached oxygen atoms, respectively [45].

3.2. Magnetic properties

The magnetic ground states of clusters are described in Figure 1 and the supplementary material [41]. Our DFT calculations imply that the ferromagnetic state is favored for most of studied clusters. The ferrimagnetic state is found for $CoCrO^+$, $Co_2CrO_2^+$, $CoCr_2O^+$, and $CoCr_2O_2^+$, where the local spin of one metal atom is in antiparallel relation to the others (see Figure 1). While a clear trend can be extracted for the geometrical property, it is not easy to define a systematic behavior of the magnetic one. It is known that Co and Cr are magnetic elements owing to their unpaired 3*d* electrons. Their clusters can have high magnetic moments due to favored parallel magnetic couplings and large per-atom spin polarization [46]. However, the oxidizing process is expected to influence the total magnetic moments of Co–Cr clusters via donating their valence electrons in metal–oxygen bonds. In addition, the occurrence of stronger metal–oxygen bonds might weaken metal–metal bonds, leading to less preferred parallel or even antiparallel magnetic couplings in certain cases [16]. These all factors, particularly the geometry, size, composition, number and position of oxygen atoms, as shown below, can influence the cluster magnetic behavior.

To get insight into the magnetism behavior of $Co_xCr_yO_m^+$ clusters, the local magnetic moment [$M(\mu_B)$] on each atom for the ground state structures are calculated and presented in Figure 2 as a function of oxygen concentration. A few general comments about the cluster magnetic behavior can be made with relation to their electronic and geometrical details. Firstly, the local magnetic moment of Cr is higher than that of Co due to the number of unpaired electron in Cr atom ($3d^54s^1$) more than in Co atom ($3d^74s^2$). Pure cobalt and chromium oxide cluster cations favor the

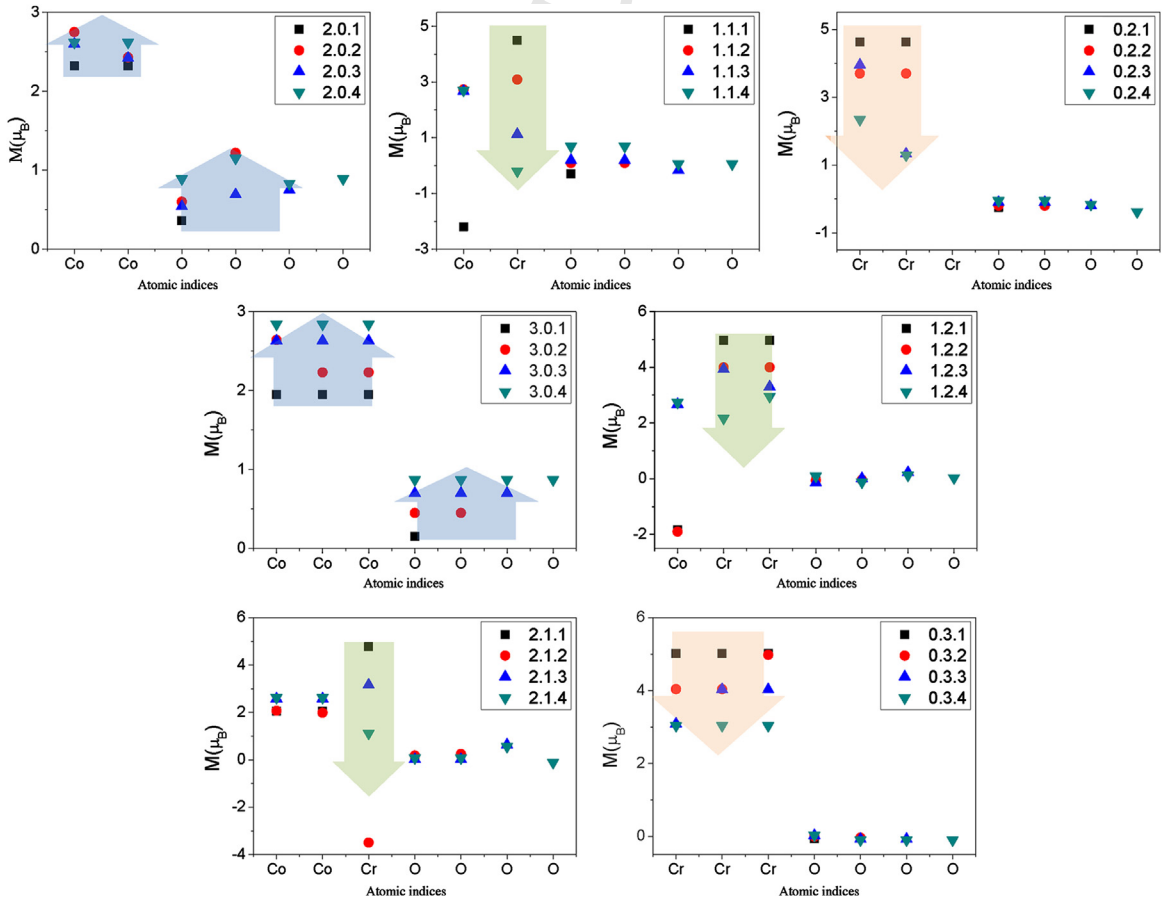

Figure 2. Calculated local magnetic moments M (μ_B) of ground state $Co_xCr_yO_m^+$ ($x+y=2$, 3 and $m=1$–4) clusters as a function of oxygen concentration. The inset values indicate the cluster composition $x.y.m$. Details of the local magnetic moment can be found in Ref. [41].

Please cite this article in press as: H.T. Pham, et al., Chem. Phys. Lett. (2015), http://dx.doi.org/10.1016/j.cplett.2015.11.015

Table 2
Calculated dissociation energies (DEs, in eV) to remove an atomic oxygen, a molecular oxygen, a Co atom, a Cr atom, a cationic Co^+, or a cationic Cr^+ atom.

Parents	DE(O)	DE(O_2)	DE(Co)	DE(Cr)	DE(Co^+)	DE(Cr^+)
Co_2O^+	5.17	–	4.28	–	3.51	–
$Co_2O_2^+$	3.31*	2.95	4.29	–	2.97	–
$Co_2O_3^+$	3.49	1.27*	4.72	–	2.98	–
$Co_2O_4^+$	3.32	1.28*	4.74	–	2.84	–
$CoCrO^+$	6.22	–	4.01	4.70	3.33	3.36
$CoCrO_2^+$	4.88*	5.58	5.16	6.28	2.89	4.39
$CoCrO_3^+$	4.34*	3.69	5.88	7.56	2.94	5.25
$CoCrO_4^+$	2.98	1.79*	5.99	7.24	2.63	4.77
Cr_2O^+	5.96	–	–	4.34	–	3.09
$Cr_2O_2^+$	5.45	5.87	–	6.06	–	3.21
$Cr_2O_3^+$	4.37	4.29	–	6.81	–	3.29
$Cr_2O_4^+$	4.09	2.92*	–	8.02	–	4.09
Co_3O^+	5.03	–	2.52	–	3.38	–
$Co_3O_2^+$	4.73*	4.23	3.93*	–	3.33	–
$Co_3O_3^+$	5.48	4.68*	5.92	–	4.70	–
$Co_3O_4^+$	2.33*	2.28	4.93	–	3.84	–
Co_2CrO^+	6.33	–	2.35	2.77	3.60	3.06
$Co_2CrO_2^+$	5.57	6.38*	3.04	5.03	3.43	3.86
$Co_2CrO_3^+$	5.40	5.44*	4.10	6.95	3.43	4.95
$Co_2CrO_4^+$	4.37	4.24*	5.49	7.99	3.17	6.33
$CoCr_2O^+$	6.30	–	2.17	2.51	3.41	3.18
$CoCr_2O_2^+$	5.81	6.59	2.54	3.44	3.73	3.26
$CoCr_2O_3^+$	5.48	5.76	3.65	4.58	3.12	3.33
$CoCr_2O_4^+$	4.81	4.76	4.38	6.41	2.89	3.51
Cr_3O^+	6.47	–	–	2.40	–	3.07
$Cr_3O_2^+$	5.80	6.74	–	2.75	–	3.36
$Cr_3O_3^+$	6.06	6.32	–	4.44	–	3.34
$Cr_3O_4^+$	5.44	5.97	–	5.79	–	3.73

* Experimentally preferred channels [27,36,45,52].

parallel magnetic couplings while doped species show an oscillatory magnetic behavior. Importantly, the total magnetic moments of clusters are simultaneously governed by their electronic and geometric properties. In particular, the number of unpaired electrons in a Co atom increases while that in a Cr atom reduces by donating electrons to Co–O bonds. This leads to the fact that increasing oxygen concentration gradually empties the more than half-filled $3d^74s^2$ shell in Co atoms, consequently enhancing their local magnetic moments. On the other hand, the local magnetic moment of Cr atoms reduces under oxidation because of gradually emptying the half-filled $3d^54s^1$ shell. It is in line with the observation that the local magnetic moment of Co atoms increases (blue arrows in Figure 2) but that of Cr atoms decreases as increasing the number of metal-*oxygen bonds (orange arrows in Figure 2). In detail, the ground state magnetic moment of $Co_2O_m^+$ and $Co_3O_m^+$ increases from 5 to 9μ_B and from 6 to 12μ_B when m goes from 1 to 4, respectively. Meanwhile, the ground state magnetic moment of $Cr_2O_m^+$ and $Cr_3O_m^+$ goes down from 9 to 3μ_B and from 15 to 9μ_B, respectively. Even in a cluster, the dependence of local magnetic moments on the number of metal–oxygen bonds is obvious. For instance, Co and O atoms in the symmetric ring $Co_3O_3^+$ have the same local magnetic moment because each shares a pair of Co–O bonds. Meanwhile, for $Co_3O_2^+$, the first Co atom has the same local magnetic moment as those in $Co_3O_3^+$ but others have only one Co–O bond, resulting in lower local magnetic moments [41]. Not only the number of metal–oxygen bonds but also the geometrical structure influences the total magnetic moment of clusters. For example, two Cr atoms bridging two O atoms in the symmetric ring $Cr_2O_2^+$ cluster have the same local magnetic moment (3.70μ_B). Nevertheless, those of two Cr atoms bridging three O atoms in $Cr_2O_4^+$ are different (1.29 and 2.34μ_B) because of its asymmetric structure. The substantial reduction in the local magnetic moment of Cr under oxidizing is in line with the previous prediction on neutral Cr_2O_n clusters [22]. Similar argument can be used to link the change in local magnetic moment and corresponding geometrical structure or coordination.

It should be mentioned that ferromagnetic $Cr_2O_3^+$ has a ground state magnetic moment of 5μ_B but a 3μ_B ferrimagnetic isomer at 0.01 eV higher in energy is observed. Degenerate isomers are also found for several doped species. These puzzling situations are due to the fact that the (parallel/anti-parallel) alignment of localized magnetic moments strongly depends on the unpaired 3d electrons. These electrons do not participate in the metal–oxygen chemical bonds and are easily affected by the surrounding electronic environment (created by oxygen or other metal atoms), which can cause a change in alignment of local spins readily. For instance, the total magnetic moment of $CoCrO_3^+$ can be either 4μ_B (ground state) or 2μ_B (+0.02 eV). The ground state magnetic moment of $CoCrO_4^+$ is 4μ_B while its next isomer requires a relative excess energy of 0.04 eV with the magnetic moment of 2μ_B. Similarly, though for $CoCr_2O^+$ the ferrimagnetic ground state moment of 8μ_B is found, a ferromagnetic state with 12μ_B is located 0.01 eV higher in energy. It is interesting that the successive addition of oxygen in doped oxide clusters leads to an obvious reduction of the localized magnetic moments at Cr sites (green arrows) while the local magnetic moments of Co atoms slightly increase (from 2.3 to 2.8μ_B). This difference between M(Cr) and M(Co) implies that (i) cobalt atoms bond weakly to oxygen ones and (ii) the doped oxide clusters are mainly governed by strong Cr–O bonds. This is also in line with the further investigation on the dissociation channels of alloy oxide species (Table 2), where the loss of Co/Co^+ is most preferred. Although M(Co) seems to be unchanged in magnitude, it oscillates from positive to negative, leading to ferrimagnetic couplings at certain cases, e.g. $CoCrO^+$, $CoCr_2O^+$, and $CoCr_2O_2^+$. Cr atom also gets anti-ferromagnetically aligned in the $Co_2CrO_2^+$ cluster. These ferromagnetic-to-ferrimagnetic transitions can be related to complex progression of the chemical bonding imbalance between Cr–O and Co–O [47], which induces the opposite spin polarization by forming minority orbitals lying below the Fermi energy. Apparently, the appearance of antiparallel magnetic couplings makes the magnetic behavior of doped clusters strongly oscillated, showing no systematical trend.

Please cite this article in press as: H.T. Pham, et al., Chem. Phys. Lett. (2015), http://dx.doi.org/10.1016/j.cplett.2015.11.015

3.3. Dissociation energies and relative stability

The dissociation energy reflects the intrinsic stability of clusters while the dissociation channel is often governed by relative stabilities of daughter clusters [27,45,48–52]. Clusters requiring a higher dissociation energy are relatively more stable than others. The evaporation processes tend to terminate at the fragment with enhanced stability. In the followings, we calculate the dissociation energies (DEs) of $Co_xCr_yO_m^+$ ($x+y=2$, 3 and $m=1$–4) clusters for selected potential dissociation channels. Table 2 presents the DEs (in eV) to remove atomic oxygen, molecular oxygen, a Co atom, a Cr atom, a Co^+ cation, or a Cr^+ cation. In our calculations, those energies are obtained by assuming lowest energy structures and spin states for the parents and the fragments. With the applied DFT functional level, a uncertainty of about ±0.3 eV on thermodynamic parameters is expected.

For the group $x+y=2$, the mono-oxide clusters prefer emitting a cationic metal atom. In particular, Co_2O^+, $CoCrO^+$, and Cr_2O^+ likely dissociate via either a Co^+ or Cr^+ ion. This could relate to their corresponding ground-state structures, where a larger dissociation energy might be required for breaking metal–oxygen–metal bonds to deliver oxygen fragments. For higher oxygen concentrations, the dissociation channel of $Co_2O_2^+$ could be via the evaporation of either O (3.31 eV), O_2 (2.95 eV), or Co^+ (2.97 eV). Meanwhile, DEs (O_2) of $Co_2O_3^+$ and $Co_2O_4^+$ (1.27 and 1.28 eV, respectively) are remarkably lower than those of the other channels, implying the relatively high stability of Co_2O^+ and $Co_2O_2^+$. Similarly, the most preferable dissociation channels for $CoCrO_4^+$, and $Cr_2O_4^+$ are to decay through the loss of an oxygen molecule. Therefore, a same argument can be applied for stable $CoCrO_2^+$ and $Cr_2O_2^+$ clusters when DEs (O_2) of $CoCrO_4^+$ and $Cr_2O_4^+$ (1.79 and 2.92 eV, respectively) are relatively lower than others. The lowest-energy dissociation channels of alloy oxide clusters $CoCrO_2^+$ and $CoCrO_3^+$ are via Co^+ emission. $Cr_2O_{2,3}^+$ clusters are predicted to be dissociate via Cr^+ emission. The remarkably higher dissociation energy (2.92 eV) of $Cr_2O_4^+$ suggests its enhanced stability over those of the same size clusters (1.28 eV for $Co_2O_4^+$ and 1.79 eV for $CoCrO_4^+$).

In contrary to $x+y=2$ mono-oxide clusters, the evaporation of a neutral metal atom is energetically preferred for $x+y=3$ species. For instance, Co_3O^+, Co_2CrO^+, and $CoCr_2O^+$ favor the loss of a Co atom while Cr_3O^+ decays via the Cr atom evaporation. The preference of Co atom loss in doped clusters is consistent with the higher strength of Cr–O bonds compared to that of Co–O, which is not obvious in the dissociation behavior of the $CoCrO^+$ cluster. If the charge of the parent cation cluster preferably resides on the fragment species with the lower ionization potential [53], it could lead to the ionization rules that are, for example, IP(CoO) > IP(Co_2O), IP(CoO) > IP(CoCrO), IP(CoO) > IP(Cr_2O), and IP(CrO) > IP(Cr_2O). This is in an excellent agreement with calculated ionization energies of $Co_xCr_yO_m^+$ [41], supporting why a cationic or neutral Co/Cr atom loss is favored. Except for $Co_3O_4^+$, this tendency keeps valid for higher oxygen-concentration species: dissociating via either neutral or cation metal atoms is preferred where still emitting Co^+/Co is the lowest-energy dissociation channel in alloying oxide species. $Co_3O_4^+$ cluster likely decays via the loss of O and O_2 with considerably lower DEs (2.33 and 2.28 eV, respectively) than those of the other channels, suggesting the enhanced stability of $Co_3O_2^+$ and $Co_3O_3^+$, respectively. Same conclusions for the relatively high stabilities of $CoCrO_4$ [DE(Co^+) of $Co_2CrO_4^+$ = 3.17 eV] and Cr_2O_4 [DE(Co^+) of $CoCr_2O_4^+$ = 2.89 eV, DE(Cr^+) of $Cr_3O_4^+$ = 3.73 eV].

The photofragmentation measurements have been carried out for several cluster sizes and compositions [27,36,45,52]. In Table 2, the experimentally favored channels are marked with the superscript '*' for reference. Taking the computational error margin, the calculated dissociation energies and experimental observations are in a good satisfactory. The enhanced stability of Co_2O^+, $Co_2O_2^+$, $CoCrO_2^+$, $Cr_2O_2^+$, and $Cr_2O_4^{0,+}$ is in line with experimental observation. The most surprising difference is that the evaporation of a neutral/cationic metal atom is predicted to be the lowest-energy dissociation channel for $x+y=3$ alloying species while the incomplete experiments suggested that the molecular oxygen evaporation seems to be the most facile one. One of the possible reasons could be due to the existence of transition states, which might require an activation energy to particularly remove a neutral/cationic metal atom. A detailed investigation on such energy barriers will be addressed in a separated paper. Alternatively, the discrepancy between simulation and experimental conditions should not be excluded. The over-high photodissociation energy might not guarantee that the clusters get equilibrium before the fragmentation processes take place. The possibility of hot clusters, which have an initial high internal energy and could already be excited before absorbing photons, should also be taken into account.

4. Conclusions

The structure, magnetism, and dissociation behavior of small bimetallic oxide $Co_xCr_yO_m^+$ ($x+y=2$, 3 and $1 \le m \le 4$) clusters have been studied using DFT calculations. Due to strong metal–oxygen bonding, the oxidation process evolves via two stages: in the first stage, the oxygen atoms preferably occupy all the bridging positions and in the second stage, the next oxygen atoms bind atop or aside metal atoms with a preference of Cr sites. The ferromagnetic state is observed for most of clusters except for $CoCrO^+$, $Co_2CrO_2^+$, $CoCr_2O^+$, and $CoCr_2O_2^+$, which are predicted to be ferrimagnetic. The total magnetic moments of pure cobalt oxide clusters are found to increase during the oxidation while those of chromium counterparts tend to reduce with increasing the oxygen content. The size and composition-dependent magnetic behavior of doped clusters is expressed via the ferromagnetic-to-ferrimagnetic transition, which could be induced by the chemical bonding between Cr/Co and O. The dissociation behavior is investigated, identifying the stable patterns, for instance, Co_2O^+, $Co_2O_2^+$, $CoCrO_2^+$, $Cr_2O_4^+$, Cr_2O_4, $Cr_2O_2^+$, $Co_3O_2^+$, $Co_3O_3^+$, and $CoCrO_4$. We believe our results to be of interest for designing building blocks for transition metal oxide based magnetic nanostructured materials. We also expect to motivate further photodissociation and Stern–Gerlach magnetic deflection experiments, which could deliver conclusive answers, via the comparison with our results, on the relative stability and magnetic moment of bimetallic oxide $Co_xCr_yO_m^+$ clusters.

Uncited reference

[54].

Acknowledgments

This research was supported by the Vietnam National Foundation for Science and Technology Development (NAFOSTED) under grant number 103.02-2014.67.

Appendix A. Supplementary Data

Supplementary data associated with this article can be found, in the online version, at http://dx.doi.org/10.1016/j.cplett.2015.11.015.

References

[1] G.R. Patzke, Y. Zhou, R. Kontic, F. Conrad, Angew. Chem. Int. Ed. 50 (2011) 826.
[2] J.A. Alonso, Chem. Rev. 100 (2000) 637.

[3] J. Garcia-Barriocanal, A. Rivera-Calzada, M. Varela, Z. Sefrioui, M.R. Diaz-Guillen, K.J. Moreno, J.A. Diaz-Guillen, E. Iborra, A.F. Fuentes, S.J. Pennycook, C. Leon, J. Santarnaria, ChemPhysChem 10 (2009) 1003.
[4] P.A. Cox, Transition Metal Oxides, Clarendon, Oxford, 1992.
[5] C.N. Rao, B. Raveau, Transition Metal Oxides, Wiley, New York, 1998.
[6] K.R. Asmis, Phys. Chem. Chem. Phys. 14 (2012) 9270.
[7] E. Janssens, G. Santambrogio, M. Brummer, L. Woste, P. Lievens, J. Sauer, G. Meijer, K.R. Asmis, Phys. Rev. Lett. 96 (2006) 233401.
[8] B. Helmich, M. Sierka, J. Dbler, J. Sauer, Phys. Chem. Chem. Phys. 16 (2014) 8441.
[9] Y. Wang, Q. Zhou, M. Yang, J. Wang, Comp. Theo. Chem. 1021 (2013) 262.
[10] H.J. Zhai, X. Huang, T. Waters, X.B. Wang, R.A.J. O'Hair, A.G. Wedd, L.S. Wang, J. Phys. Chem. A 109 (2005) 10512.
[11] N.J. Mayhall, D.W. Rothgeb, E. Hossain, K. Raghavachari, C.C. Jarrold, J. Chem. Phys. 130 (2009) 124313.
[12] J.E. Mann, D.W. Rothgeb, S.E. Waller, C.C. Jarrold, J. Phys. Chem. A 114 (2010) 11312.
[13] J.E. Mann, S.E. Waller, C.C. Jarrold, J. Chem. Phys. 137 (2012) 044301.
[14] S.E. Waller, J.E. Mann, D.W. Rothgeb, C.C. Jarrold, J. Phys. Chem. A 116 (2012) 9639.
[15] L. Jiang, T. Wende, P. Claes, S. Bhattacharyya, M. Sierka, G. Meijer, P. Lievens, J. Sauer, K.R. Asmis, J. Phys. Chem. A 115 (2011) 11187.
[16] M.B. Torres, A. Aguado, F.A. Granja, A. Vega, L.C. Ballás, J. Phys. Chem. C (2015), http://dx.doi.org/10.1021/jp5121349.
[17] Y. Matsumoto, M. Murakami, T. Shono, T. Hasegawa, T. Fukumura, M. Kawasaki, P. Ahmet, T. Chikyow, S.Y. Koshihara, H. Koimura, Science 291 (2001) 854.
[18] K.A. Griffin, A.B. Pakhomov, C.M. Wang, S.M. Heald, K.M. Krishnan, Phys. Rev. Lett. 94 (2005) 157204.
[19] I.S. Elfimov, A. Rusydi, S.I. Csiszar, Z. Hu, H.H. Hsieh, H.J. Lin, C.T. Chen, R. Liang, G.A. Sawatzky, Phys. Rev. Lett. 98 (2007) 137202.
[20] H. Pan, J.B. Yi, L. Shen, R.Q. Wu, J.H. Yang, J.Y. Lin, Y.P. Feng, J. Ding, L.H. Van, J.H. Yin, Phys. Rev. Lett. 99 (2007) 127201.
[21] R. Long, N. English, Phys. Rev. B 80 (2009) 115212.
[22] B.V. Reddy, S.N. Khanna, Phys. Rev. Lett. 83 (1999) 3170.
[23] K. Tono, A. Terasaki, T. Ohta, T. Kondow, Phys. Rev. Lett. 90 (2003) 133402.
[24] W. Eerenstein, N.D. Mathur, J.F. Scott, Nature 442 (2006) 759.
[25] Y. Yamasaki, S. Miyasaka, Y. Kaneko, J.P. He, T. Arima, Y. Tokura, Phys. Rev. Lett. 96 (2006) 207204.
[26] Y.J. Choi, J. Okamoto, D.J. Huang, K.S. Chao, H.J. Lin, C.T. Chen, M. van Veenendaal, T.A. Kaplan, S.W. Cheong, Phys. Rev. Lett. 102 (2009) 067601.
[27] N.T. Tung, N.M. Tam, M.T. Nguyen, P. Lievens, E. Janssens, J. Chem. Phys. 141 (2014) 044311.
[28] S. Yin, R. Moro, X. Xu, W.A. de Heer, Phys. Rev. Lett. 98 (2007) 113401.
[29] U. Rohrmann, R. Schäfer, Phys. Rev. Lett. 111 (2013) 133401.
[30] N.T. Tung, Stability of Bimetallic Clusters and Development of a Magnetic Deflection Setup (PhD Thesis), KU Leuven, 2014.
[31] A.D. Becke, J. Chem. Phys. 98 (1993) 5648.
[32] J.P. Perdew, Phys. Rev. B 33 (1986) 8822.
[33] M.J. Frisch, et al., Gaussian 09, Revision B. 01, Gaussian, Inc, Wallingford CT, 2009.
[34] T.B. Tai, M.T. Nguyen, J. Chem. Theo. Comput. 7 (2011) 1119.
[35] L. Liu, R.N. Zhao, J.G. Han, F.Y. Liu, G.Q. Pan, L.S. Sheng, J. Phys. Chem. A 113 (2009) 360.
[36] G.E. Johnson, J.U. Reveles, N.M. Reilly, E.C. Tyo, S.N. Khanna, A.W. Castleman Jr., J. Phys. Chem. A 112 (2008) 11330.
[37] E. Uzonova, G. St Nikolov, H. Mikosch, J. Phys. Chem. A 106 (2002) 4104.
[38] Y.R. Luo, Comprehensive Handbook of Chemical Bond Energies, CRC Press, Boca Raton, FL, 2007.
[39] R.R. Reddy, Y.N. Ahammed, K.R. Gopal, P.A. Azeem, S. Anjaneyulu, Astrophys. Space Sci. 262 (1998) 223.
[40] G.L. Gutsev, P. Jena, H.J. Zhai, L.S. Wang, J. Chem. Phys 115 (2001) 7935.
[41] Supplementary material for optimized structures of energetically low-lying isomers.
[42] S. Datta, M. Kabir, T. Saha-Dasgupta, A. Mookerjee, Phys. Rev. B 80 (2009) 085418.
[43] N. Shen, Y. Wang, S. Chen, J. Wang, Front. Phys. China 4 (2009) 408.
[44] S. Yin, W. Xue, X.L. Ding, W.G. Wang, S.G. He, M.F. Ge, Int. J. Mass Spec. 281 (2009) 72.
[45] K.S. Molek, Z.D. Reed, A.M. Ricks, M.A. Duncan, J. Phys. Chem. A 111 (2007) 8080.
[46] S. Yin, R. Moro, X. Xu, W.A. de Heer, Phys. Rev. Lett. 98 (2007) 113401.
[47] B.V. Reddy, S.N. Khana, C. Ashman, Phys. Rev. B 61 (2000) 5797.
[48] L. Schweikhard, K. Hansen, A. Herlert, M.D. Herraiz Lablanca, M. Vogel, Eur. Phys. J. D 36 (2005) 179.
[49] N. Veldeman, E. Janssens, K. Hansen, J. De Haeck, R.E. Silverans, P. Lievens, Faraday Discuss. 138 (2007) 147.
[50] S. Bhattacharyya, T.T. Nguyen, J. De Haeck, K. Hansen, P. Lievens, E. Janssens, Phys. Rev. B 87 (2013) 054103.
[51] J.B. Jaeger, T.D. Jaeger, M.A. Duncan, J. Phys. Chem. A 110 (2006) 9310.
[52] C.J. Dibble, S.T. Akin, S. Ard, C.P. Fowler, M.A. Duncan, J. Phys. Chem. A 116 (2012) 5398.
[53] Assuming that the photofragmentation takes place on the ground-state potential energy surface.
[54] N.T. Tung, E. Janssens, P. Lievens, Appl. Phys. B 114 (2014) 497.

Please cite this article in press as: H.T. Pham, et al., Chem. Phys. Lett. (2015), http://dx.doi.org/10.1016/j.cplett.2015.11.015